Hot electron production and diffuse excited states in C70, C82, and Sc3N@C80 characterized by angular-resolved photoelectron spectroscopy

Hot electron production and diffuse excited states in C70, C82, and Sc3N@C80 characterized by angular-resolved photoelectron spectroscopy

J. Olof Johansson, Elvira Bohl, Gordon G. Henderson, Benoit Mignolet, T. John S. Dennis, Francoise Remacle, and Eleanor E. B. Campbell

Citation: The Journal of Chemical Physics **139**, 084309 (2013); doi: 10.1063/1.4818987
View online: http://dx.doi.org/10.1063/1.4818987
View Table of Contents: http://scitation.aip.org/content/aip/journal/jcp/139/8?ver=pdfcov
Published by the AIP Publishing

Hot electron production and diffuse excited states in C_{70}, C_{82}, and $Sc_3N@C_{80}$ characterized by angular-resolved photoelectron spectroscopy

J. Olof Johansson,[1] Elvira Bohl,[1] Gordon G. Henderson,[1] Benoit Mignolet,[2] T. John S. Dennis,[3] Francoise Remacle,[2] and Eleanor E. B. Campbell[1,a)]
[1]*EaStCHEM, School of Chemistry, University of Edinburgh, Edinburgh EH9 3JJ, United Kingdom*
[2]*Département de Chimie, B6c, Université de Liège, B4000 Liège, Belgium*
[3]*School of Physics and Astronomy, Queen Mary University of London, Mile End Road, London E1 4NS, United Kingdom*

(Received 1 July 2013; accepted 5 August 2013; published online 27 August 2013)

Angular-resolved photoelectron spectroscopy using wavelength-tuneable femtosecond laser pulses is presented for a series of fullerenes, namely, C_{70}, C_{82}, and $Sc_3N@C_{80}$. The photoelectron kinetic energy distributions for the three molecules show typical thermal electron spectra with a superimposed peak structure that is the result of one-photon ionization of diffuse low-angular momenta states with electron density close to the carbon cage and that are related to so-called super atom molecular orbitals. Photoelectron angular distributions confirm this assignment. The observed structure is less prominent compared to the thermal electron background than what was observed in C_{60}. It can be concluded that hot electron emission is the main ionization channel for the larger and more complex molecules for these excitation conditions. © *2013 AIP Publishing LLC*. [http://dx.doi.org/10.1063/1.4818987]

I. INTRODUCTION

A fundamental understanding of the electronic structure and photoinitiated electron dynamics in large organic molecules and carbon nanomaterials is important for optimizing their properties for use in molecular electronics and organic photovoltaics. C_{60} is an excellent model system for acceptor molecules, such as $PC_{60}BM$, due to its high symmetry and simple chemical composition, which simplifies theoretical modelling.[1] Photoelectron spectroscopy studies of gas-phase fullerenes after ca. 100 fs laser excitation have shown that an efficient energy redistribution produces hot electrons leading to the emission of thermal electrons with a characteristic Boltzmann-like photoelectron spectrum (PES).[2] Superimposed on the thermal electron background, a series of clear peaks converging on the ionization energy can be observed that were initially assigned to one-photon ionization of Rydberg states with large orbital angular momenta ($\ell = 3$, 5, and 7).[3] Photoelectron angular distributions (PADs) have been shown to be a powerful tool to clearly identify the states giving rise to some of this peak structure in PES and could, in combination with a recent computational study by Mignolet *et al.*, show that the peak structure seen in fs spectra is due to excitation of diffuse, excited states.[4,5] These diffuse states are Rydberg-like states with low orbital angular momenta ($\ell = 0$, 1, and 2)[4] and at least two radial nodes in the wavefunction ($n = 3$). The lowest-lying s-state predominantly consists of the excitation of the s "Super Atom Molecular Orbital" (s-SAMO) that was originally studied by Feng *et al.*[6] using scanning tunnelling spectroscopy of fullerenes supported on metal substrates. Higher-lying states, such as the p and d states, are further away from the core, in contrast to the s-SAMO, and therefore show a mixture of SAMO and more conventional Rydberg character, where the long range Coulomb force dominates the interaction.[5] It is not clear how much of the SAMO-character is retained in larger and more complex fullerenes, although there have been a few studies, mainly theoretical, that have identified SAMOs in systems other than C_{60}.[7,8]

Recently, Grancini *et al.*[9] found that in a solar cell composed of a polymer donor and $PC_{60}BM$ acceptor, above-gap excitation in the donor produces hot, delocalised interfacial charge transfer states that result in much more efficient charge dissociation. The diffuse SAMOs, giving rise to nearly free-electron bands in solids,[7] could potentially play a key role in the diffuse charge transfer states mediating the efficient charge dissociation observed.[9] A deeper understanding of the nature of the excited states and the hot electron dynamics in model acceptor materials may therefore lead to improved light-harvesting devices.

To probe the influence of molecular size and symmetry on both the thermal electron emission and diffuse excited states, we have carried out measurements on a series of fullerenes with lower symmetry than C_{60}, namely, C_{70}, C_{82}, and the endohedral fullerene $Sc_3N@C_{80}$. Experimentally, gas-phase studies are ideally suited for understanding the fundamental aspects of these states, since there are no solvents or surfaces present that perturb the electronic structure. The paper is organized as follows. In Sec. II, the experimental setup is briefly described and we show how binding energies and PADs are extracted from the measurements. We also briefly describe the computational methodology used

a)Author to whom correspondence should be addressed. E-mail: eleanor.campbell@ed.ac.uk.

to compute the excited states and compare with the experimental binding energies. In Sec. III, PES with clear thermal electron signatures are presented for the molecules studied. Subsequently, the focus is shifted to assigning the peaks superimposed on the thermal background, which is possible by comparing to results for C_{60}. PES and PADs are therefore first presented for C_{60} and then for C_{70}, C_{82}, and $Sc_3N@C_{80}$.

II. METHODS

A. Experimental setup

The experimental setup is similar to the one presented in Ref. 10. Neutral gas-phase fullerenes from purified powder of C_{60}, C_{70}, C_{82}, and $Sc_3N@C_{80}$ were prepared from an effusive oven at a temperature of ca. 500 °C inside a vacuum chamber with pressure below 10^{-8} mbar. The output from a non-collinear optical parametric amplifier (NOPA), pumped by a regenerative titanium sapphire amplifier (producing 800 nm, 120 fs laser pulses of 3.8 mJ pulse energy), was passed into the vacuum chamber at right angles to the effusive molecular beam. The pulse duration after passing through a half-wave plate, Glan-laser polarizer, and a vacuum viewport was approximately 90 fs. The wavelength range used from the NOPA was 500–750 nm, but was complimented by the fundamental and second harmonic of the regenerative amplifier (800 and 400 nm, respectively). Mass spectra were collected with a time-of-flight mass spectrometer. For all spectra presented in this paper, the laser power was adjusted so that the lowest possible detectable signal was obtained, which typically meant that only singly charged molecular parents were observed. Typical mass spectra are shown in Figure 1. The intact molecular ion was the most abundant species in the mass spectra, although for C_{82} a small fraction of C_{84} was observed as well. The electrons were extracted onto a position sensitive detector consisting of a pair of microchannel plates and a phosphor screen using a standard velocity-map imaging (VMI) electrode configuration.[11] The resulting VMI images were inverted using a modified version of Polar Onion-Peeling (POP)[12] that included up to the tenth Legendre polynomial in the inversion procedure.

B. Data analysis

Data collected using 120 fs, 400 nm, and 1.1 TW cm^{-2} intensity are presented in Figure 2 for C_{60}. For this pulse duration and intensity, the PES typically show thermal electron emission, as characterized by an exponential kinetic energy distribution.[13] A series of peaks can be seen superimposed on the thermal electron background, and in order to extract angular distributions for these peaks, it is first necessary to remove the thermal electron background. We do this by dividing the inverted VMI image into 10° angular segments, which is shown in Figure 2 for the segments corresponding to 0°–10° (parallel to the laser polarization direction), 40°–50°, and 80°–90° (perpendicular to the laser polarization direction). Clear peaks are observed along the laser polarization direction for this wavelength. Perpendicular to the laser polarization direction, an exponential distribution is observed (plotted in log-lin scale) due to thermal electron emission, although some residual peak structure is still visible. An exponential distribution is fitted to the 80°–90° angular segment and subsequently subtracted from all other angular segments. For longer wavelengths and higher intensities, the thermal electron background becomes asymmetric because of the laser field's influence on the emitted electrons,[13] which complicates the thermal background subtraction. Also, above-threshold ionization (ATI) peaks superimposed on the

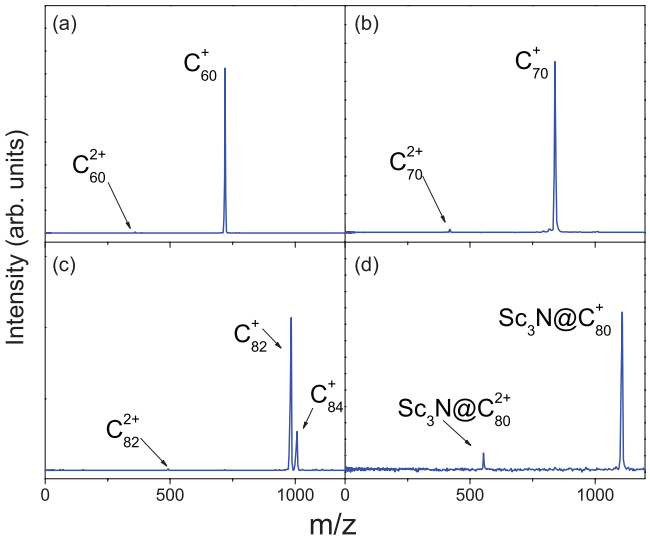

FIG. 1. Mass spectra obtained for the different molecules (indicated in the figure) with typical laser excitation conditions where the intact molecular ion is the dominant species in the mass spectrum. The laser wavelengths and intensities were (a) 500 nm, 4.7 TW cm^{-2}; (b) 520 nm, 2.9 TW cm^{-2}; (c) 519 nm, 2.8 TW cm^{-2}; and (d) 506 nm, 4.1 TW cm^{-2}. The pulse duration was approximately 90 fs.

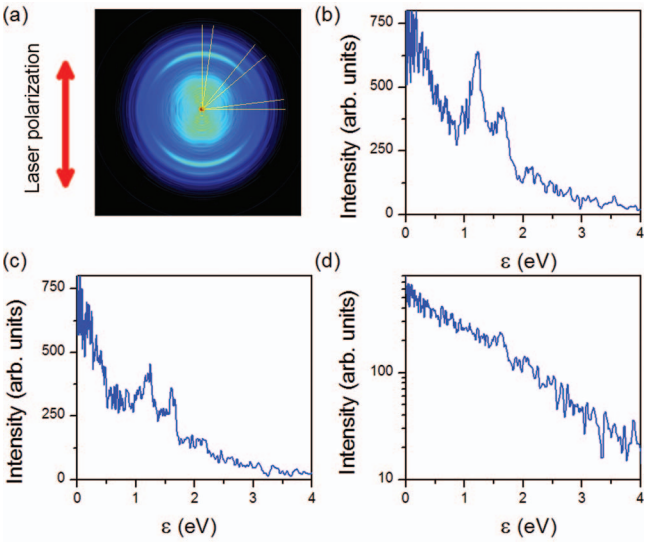

FIG. 2. (a) Inverted VMI image obtained after ionizing C_{60} with 120 fs, 400 nm laser excitation of 1.1 TW cm^{-2} (weighted by the radius for display purposes). ε is the electron kinetic energy. The yellow lines represent the angular segments that the image is divided into for producing the PES along the (b) 0°–10°, (c) 40°–50°, and (d) 80°–90° angular segments. Note that the perpendicular segment (80°–90°) is plotted in log-lin scale to emphasise the (exponential) thermal electron background.

TABLE I. Computed binding energies of the lowest SAMO states of C_{60}.

Functional	Basis	s-state E_{bind} (eV)	p-state E_{bind} (eV)	d-state E_{bind} (eV)
B3LYP	6-31 + G(d)	2.14	1.26	0.77
CAM-B3LYP	6-31 + G(d)	2.10	1.14	0.62
CAM-B3LYP	6-31 + G(d) + diffuse functions (Mignolet *et al.*[5])	2.35	1.46–1.72	1.14–1.35

background further obscure the thermal signal.[2,14] Therefore, for longer wavelengths (approximately >650 nm), where a higher intensity is needed due to a lower value of the photon absorption cross-section, an exponential distribution is fitted for each angular segment. By keeping the laser power to a minimum, however, the asymmetric effects are also kept to a minimum.

Once the thermal background has been subtracted, Lorentzian peaks are fitted to the spectra and the peak intensity vs. angle can be used to extract the angular distributions for each peak. We have found, using pulses of the order of 100 fs, that most angular distributions are very simple. In fact, we can fit the PADs with an equation used for single-photon ionization of a randomly distributed sample[15]

$$I(\theta) \propto [1 + \beta P_2(\cos\theta)], \quad (1)$$

where θ is the emission angle with respect to the laser polarization direction and P_2 is a second order Legendre polynomial that is weighted by the anisotropy parameter β (which can range from −1 to 2). Typically, Legendre polynomials of order up to $2n$ are needed to describe the PAD from a multiphoton process, where n is the number of photons involved in the ionization process.[16] Given the ionization potential of C_{60}, one would expect a polynomial order up to at least 10 for 800 nm ionization. Of course, it is possible to fit the PADs to higher order Legendre polynomials, however, including higher orders does not significantly improve the fits. The coefficient for the fourth Legendre polynomial is typically less than 10% of the fitted coefficient for the second order polynomial (i.e., the β value), which is less than the estimated 10% uncertainty in peak intensity. We therefore use Eq. (1) to fit the data. By changing the laser wavelength, it is possible to measure the kinetic energy dependence of the β-parameter for a given peak. This gives us the possibility to not only compare computed binding energies to experimental ones, but also compare the anisotropy kinetic energy dependence to calculations to assign peaks in PES.[1,4]

C. Computational details

C_{60}, C_{70}, and C_{84} (D_2 isomer) were optimized without imposing symmetry at the B3LYP/6-31+G(d) level. The geometries of C_{60}, C_{70}, and C_{84} were found to belong to the I_h, D_{5h}, and D_2 point groups, respectively. The excited states were computed by time-dependent density functional theory (TD-DFT) at the TD-DFT/B3LYP/6-31+G(d) level for a band of 500 excited states above the ground state, with symmetry imposed. All computations were carried out with GAUSSIAN 09.[17]

The functional B3LYP and the 6-31+G(d) basis set were selected in order to be able to carry out a systematic study of the SAMO states of increasingly large fullerenes. Functionals corrected for long-range electronic interactions, like the functional CAM-B3LYP used in Mignolet *et al.*,[5] are better suited for describing highly excited states with a diffuse character. However, the computation of the correction term of CAM-B3LYP increases significantly the computation time and slows down the convergence, which precludes its use for the larger fullerenes C_{70} and C_{84} when a band of 500 excited states is needed. The use of a smaller basis set, compared to what was used previously[5] for C_{60}, is motivated by the same considerations. The present basis set is large enough to describe the lower-lying SAMOs of the three fullerenes computationally investigated in this study and therefore allows for a systematic comparison of their binding energies. For C_{60}, we were able to compute the binding energies in B3LYP and CAM-B3LYP for two basis sets (see Table I). With the 6-31+G(d) basis set, the B3LYP binding energies are slightly higher than the CAM-B3LYP binding energies but the energy differences between the states remain similar (within 0.1 eV). The addition of diffuse functions increases the binding energies,[5] but overall the energetic order of the lowest SAMO states is stable. In addition, the computed photoelectron angular distributions, which strongly depend on the symmetry properties of the SAMO states, do not change substantially when using the smaller basis set. The same is true of the anisotropy parameter, β. The SAMOs of C_{70} do not exhibit a spherical symmetry but rather a cylindrical one. Therefore, the p and d manifolds of the SAMOs in C_{70} are not exactly degenerate. The p_z-SAMO orbital is lower in energy than the p_x and p_y ones, and the d_{z2} SAMO is lower than d_{zx} and d_{zy} that are, in turn, lower than d_{xy} and d_{x2-y2}.

A detailed description of the calculations of PADs was presented previously.[5] The PADs for C_{60} and C_{70} were computed for a randomly oriented sample by rotating the molecular frame of the molecule to obtain a random orientation with respect to the laboratory frame. The computed PADs were subsequently analysed using Eq. (1) to obtain the β-parameters which were then compared to experiments.

III. RESULTS AND DISCUSSION

A. Thermal electron emission

Thermal electron emission from fullerenes has previously only been studied in C_{60}, C_{70}, and, to a much lesser extent, La@C_{82} after 800 nm excitation.[10,18] The resulting PES show an exponential background distribution $I(\varepsilon) \propto \exp(-\varepsilon/k_B T_a)$, characterised by an apparent temperature

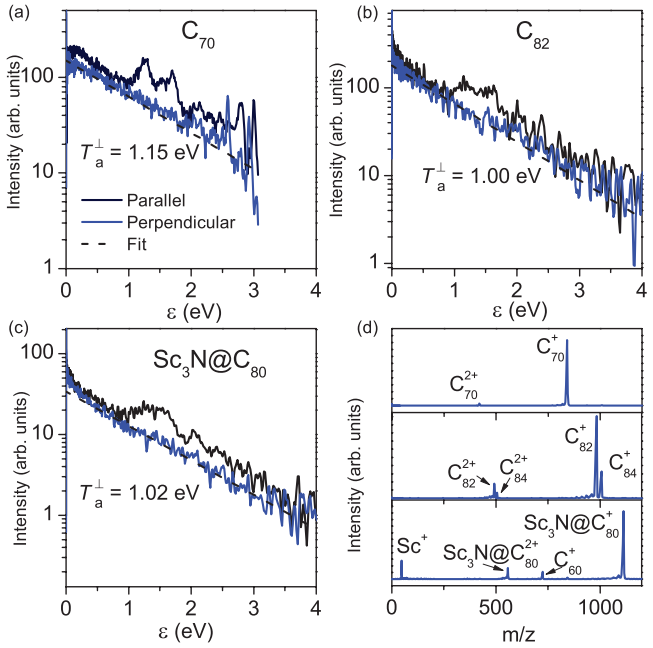

FIG. 3. PES along and perpendicular to the laser polarisation direction obtained after 400 nm, 120 fs for (a) C_{70}, 6.4 TW cm^{-2}; (b) C_{82}, 6.3 TW cm^{-2}; and (c) $Sc_3N@C_{80}$, 8.4 TW cm^{-2}. The spectrum in (a) was obtained under slightly different VMI extraction conditions to what is normally used and so the spectrum is only reliable up to ca. 2.5 eV. The corresponding mass spectra are presented in (d).

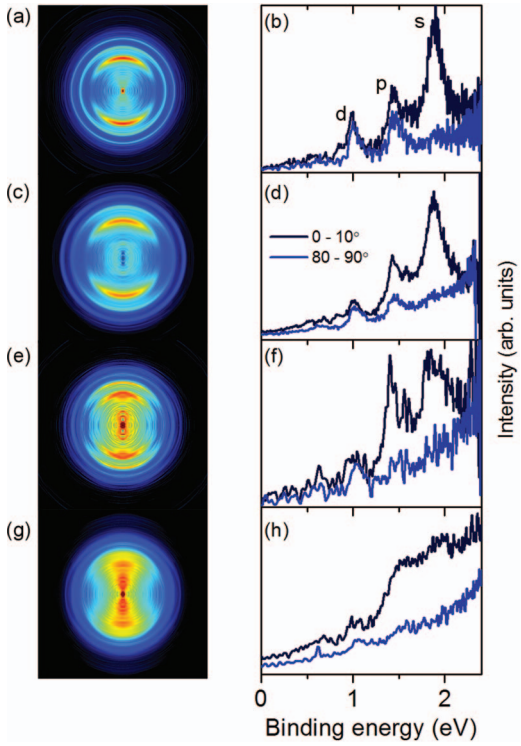

FIG. 4. Inverted VMI images and angle-resolved PES parallel and perpendicular to the laser polarization direction for [(a) and (b)] C_{60} excited with 500 nm, 4.7 TW cm^{-2}; [(c) and (d)] C_{70} excited with 520 nm, 2.9 TW cm^{-2}; [(e) and (f)] C_{82} excited with 519 nm, 2.8 TW cm^{-2}; and [(g) and (h)] $Sc_3N@C_{80}$ excited with 506 nm, 4.1 TW cm^{-2}.

T_a (k_B is Boltzmann's constant).[1,19] Angular-resolved PES, together with the corresponding mass spectra, obtained for C_{70}, C_{82}, and $Sc_3N@C_{80}$ after 120 fs, 400 nm excitation are presented in Figure 3. The spectra can, just as shown previously in the case of C_{60} and C_{70},[10] be fitted to an exponential distribution for all wavelengths studied, indicating a thermal ionization mechanism. The fitted apparent temperatures perpendicular to the laser polarization direction ($T_a^{\perp}$) are similar for all molecules, verifying the thermal nature of the electron signal, since the temperature should only be weakly dependent on the excitation spectrum of each molecule. The C_{70} temperatures are higher than for the other molecules studied here but that can be expected, since fewer electrons result in a lower heat capacity, which in turn results in higher apparent temperatures for similar excitation intensities, as is the case for C_{60}/C_{70}.[10] The results provide further evidence that efficient redistribution of excitation energy leading to thermal electron emission is a dominant ionization mechanism in fullerenes after fs laser excitation. Interestingly, this has also been shown to be the case for polycyclic aromatic hydrocarbons (PAHs),[20] which demonstrates that rapid electron thermalization occurs in a large range of organic molecules and carbon nanomaterials.

B. Identification of SAMOs

To assign the peaks observed superimposed on the thermal background in Figure 3, it is useful to compare to C_{60}, since angular-resolved photoelectron spectroscopy has been successful in identifying excited states due to the high symmetry of this molecule, leading to an almost atomic-like behaviour of the PADs with clear signatures of s- and p-states.[4] Therefore, an inverted VMI image and the corresponding angular-resolved PES parallel and perpendicular to the laser polarization direction are shown in Figures 4(a) and 4(b) for C_{60} after 500 nm, 4.7 TW cm^{-2} laser excitation. Three peaks clearly stand out and are labelled according to the assignment made in Refs. 4 and 5, namely, s-, p-, and d-states. The rich peak structure converging on the ionization energy,[3] corresponding to higher-lying states, is not resolved in this particular spectrum as the peaks become more densely spaced and the spectrometer resolution decreases with increasing kinetic energy (corresponding to decreasing binding energy in Figure 4). The Rydberg/SAMO states have orders of magnitude higher photoionization rates (of the order of 10^{14} s^{-1}) than those of the more localized valence states (with ionization rates of the order of 10^{10} s^{-1}), and will therefore ionize much more efficiently during the ca. 100 fs laser pulse, which is the reason why these particular states are observed in the fs PES.[5] The large overlap between the neutral and ionic states implies that the vibrational energy is conserved upon ionization, in analogy with Rydberg fingerprint spectroscopy,[21] which produces clear peak structure despite the high vibrational temperature at which the molecules are typically prepared experimentally. The peak structure is independent of wavelength and intensity, as is the case for the "fingerprint spectra" presented in this work. In Rydberg fingerprint spectroscopy, a highly excited state is initially populated and through internal conversion (IC), a large range of states is subsequently populated.[21–23] As soon as a SAMO/Rydberg state

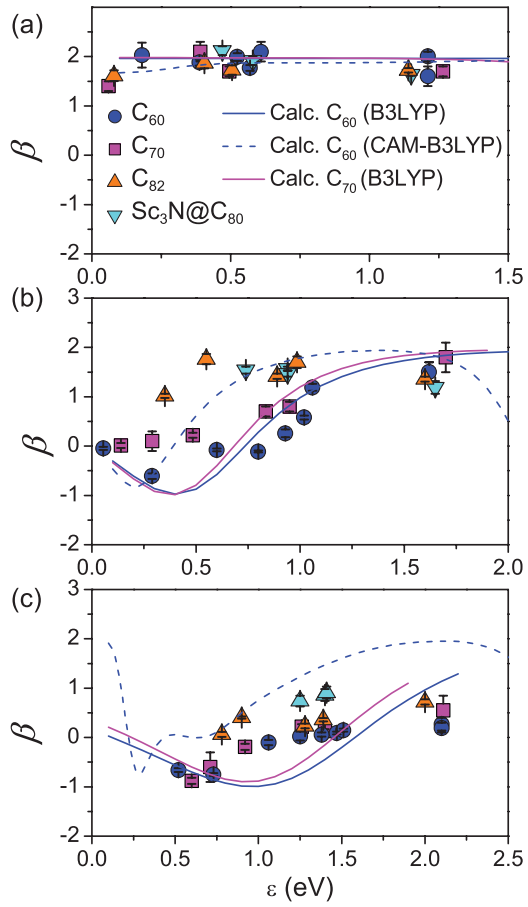

FIG. 5. Photoelectron angular distributions (PADs) for (a) s-states, (b) p-states, and (c) d-states, characterised by the fitted β value for the range of molecules studied. The lines show the calculated β-values for C_{60} and C_{70} at the TD-DFT/B3LYP/6-31+G(d) level for a randomly oriented sample (see Sec. II). The C_{60} CAM-B3LYP results from Ref. 5 are shown for comparison. Please note the difference in scale for the x-axes.

is populated through various IC processes, it will ionize due to the high ionization rate. For fullerenes in the laser interaction zone where SAMO/Rydberg states are not populated on the timescale of the laser pulse, the excited valence states do not photoionize due to the vanishingly small ionization rate, and will therefore contribute to the rapid heating of the molecules which eventually leads to hot electron production and subsequent thermal electron emission.[5]

The PADs for the three peaks, extracted from the angular dependent peak intensities, can be fitted according to Eq. (1) allowing the β-values to be extracted. The kinetic-energy dependent β-values, measured for a range of different wavelengths, are plotted in Figure 5 for the s, p, and d states. The s-state is clearly identified since $\beta \approx 2$ for all kinetic energies. The β-values for the p-state show a characteristic behaviour similar to what is calculated for the p-SAMO state.[4,5]

In Ref. 4, results for C_{70} were presented for one wavelength (400 nm). Here, we have repeated these measurements and also extended the wavelength range. The measured VMI and PES for C_{70} are very similar to C_{60} for all wavelengths measured, as shown in Figures 4(c) and 4(d) for 520 nm excitation. We have therefore assigned the three prominent peaks as s-, p-, and d-states in C_{70} as well. The binding energies are slightly lower for C_{70}, as shown in Table II. The TD-DFT computations show SAMO states in C_{70} with binding energies close to what was found for C_{60} in agreement with experiments (see Sec. II). Due to the lower symmetry of C_{70}, the calculated p-state is split into a p_z state and two degenerate p_x and p_y states. The PADs extracted from the angle-resolved PES are also similar to those of C_{60}, as seen in Figure 5. In particular, the s-state shows $\beta \approx 2$ independent of kinetic energy, which provides further support for this assignment. However, β-values for the p-state are slightly larger than for C_{60}. The calculated PADs are in reasonable agreement with the experimental values (Figure 5).

TABLE II. Summary of experimental and computed (see Sec. II) binding energies of the lowest-lying Rydberg states of the fullerenes studied.

		s-state E_{bind} (eV)	p-state E_{bind} (eV)	d-state E_{bind} (eV)
C_{60}	Expt.	1.90(1)	1.47(2)	1.02(1)
	Calc.	2.14	1.26	0.77
C_{70}	Expt.	1.86(2)	1.42(2)	0.99(3)
	Calc.	2.20	1.19–1.24	0.73–0.79
C_{82}	Expt.	1.90(4)	1.42(5)	1.03(3)
C_{84}	Calc.	2.12	1.22–1.28	0.72–0.83
$Sc_3N@C_{80}$	Expt.	1.94(5)	1.50(4)	1.04(2)

A similar set of peaks for C_{82} is observed at the same binding energies as for C_{60}, although less pronounced compared to the thermal electron background (Figures 4(e) and 4(f)). Based on the binding energies and PADs, in particular for the s-state (Figure 5), it is reasonable to assign the same set of peaks to s, p, and d states of C_{82}. Zhao *et al.* reported that the s-SAMO binding energy in C_{82} is 0.2 eV higher than in C_{60}.[7] By contrast, computations performed by us have identified SAMO-like electronic states in C_{84} at very similar energies to C_{60} and it is therefore natural to assume that the same is true for C_{82} since electronic states (TD-DFT) are more relevant than molecular orbitals (DFT) in laser spectroscopy experiments. Similarly to the difference between C_{60} and C_{70}, we observe that the PAD for the p-state of C_{82} is slightly different from that of C_{60} and C_{70}.

In our experiments on $Sc_3N@C_{80}$, bands with maxima corresponding to the peak positions observed for the other fullerenes are just discernible, as shown in Figures 4(g) and 4(h). The β-values, in particular for the s-band, are consistent with those for the other fullerenes. We have therefore assigned the peaks/bands in the spectra to the same states that are observed in the other fullerenes studied. DFT computations of $Sc_3N@C_{80}$ indicate the presence of SAMO-like orbitals with an approximate binding energy of 0.5 eV,[8] in contrast to what we present here. Similarly to C_{70} and C_{82}, the β-values for the p-band are different from C_{60} and appear to be higher and peak at a lower kinetic energy for the larger, less symmetric molecules. The difference in molecular structure is obviously not large enough to significantly influence the binding energy (Table II), however, PADs are very sensitive to small changes to the molecular potential, which could explain the difference in the PADs. Also, electron-electron correlations between the

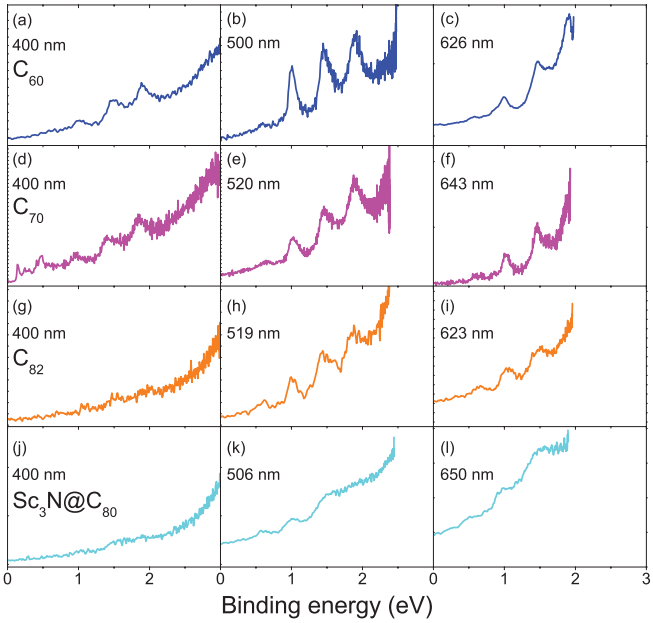

FIG. 6. Angle-integrated PES for a series of wavelength regions. Molecules and wavelengths are indicated in the figure.

outgoing electron and the residual electrons can influence the β-values, however, $\beta \approx 2$ for the s-states indicates that this is not a significant contribution for these states.

C. Angle-integrated PES

More insights are gained by comparing the angle-integrated PES, since angle-resolved spectra along a certain direction can either show a large or small contribution from a given peak depending on the β-value. Angle-integrated spectra for three typical wavelength regions are shown in Figure 6. There is a slight spread in the wavelength due to experimental conditions, however, the spectra in each region are typically very similar. As previously mentioned, the peak structure becomes less pronounced with decreasing molecular symmetry and increasing size. The underlying thermal background signal is more dominant for the larger molecules, as expected for larger particles, which will show more bulk-like properties. The binding energy does not change considerably (Table II) and it can be concluded that the binding energies of the states are not largely influenced by details of the molecular structure. This is in agreement with Rydberg Fingerprint spectroscopy that does not show a large change in binding energy of similar molecular species. This is also supported by the TD-DFT computations that do not predict a larger energy difference than what is observed experimentally.[4,5]

IV. CONCLUSIONS

In conclusion, we have presented results obtained using a combination of velocity-map imaging and Rydberg fingerprint spectroscopy to study diffuse, excited electronic states of C_{70}, C_{82}, and $Sc_3N@C_{80}$. Due to the similarity to C_{60} spectra, and, in particular, PADs characterised by $\beta \approx 2$, we have been able to assign peaks in the spectra to s-, p- and d-states. We observe an increasing thermal-to-Rydberg ratio in the spectra for increasing molecular size and complexity (but lower symmetry).

We have shown that the Rydberg fingerprint experimental technique combined with PADs has the possibility to identify potentially important diffuse states in carbon nanomaterials and complex organic molecules. The technique can also be used for probing the interplay between direct and thermal ionization and may provide important insights to help understand the electron dynamics of molecules of relevance to applications such as acceptor molecules in organic solar cells.

ACKNOWLEDGMENTS

J.O.J., E.B., and E.E.B.C. gratefully acknowledge financial support from the Leverhulme Foundation (RPF-298 "PES of hollow nanomaterials") and fruitful discussions with T. Ridley. F.R. and B.M. acknowledge support from the Fonds de la Recherche Fondamentale Collective FRFC 2.4545.12. F.R. is a Director of Research and B.M. is a PhD fellow of Fonds National de la Recherche Scientifique (FNRS, Belgium).

[1] J. O. Johansson and E. E. B. Campbell, Chem. Soc. Rev. **42**, 5661 (2013).
[2] E. E. B. Campbell, K. Hansen, K. Hoffmann, G. Korn, M. Tchaplyguine, M. Wittmann, and I. V. Hertel, Phys. Rev. Lett. **84**, 2128 (2000).
[3] M. Boyle, K. Hoffmann, C. P. Schulz, I. V. Hertel, R. D. Levine, and E. E. B. Campbell, Phys. Rev. Lett. **87**, 273401 (2001).
[4] J. O. Johansson, G. Henderson, F. Remacle, and E. E. B. Campbell, Phys. Rev. Lett. **108**, 173401 (2012).
[5] B. Mignolet, O. Johansson, E. E. B. Campbell, and F. Remacle, "Probing rapidly-ionizing super-atom molecular orbitals in C60: A computational and femtosecond photoelectron spectroscopy study," ChemPhysChem (in press).
[6] M. Feng, J. Zhao, and H. Petek, Science **320**, 359–362 (2008).
[7] J. Zhao, M. Feng, J. Yang, and H. Petek, ACS Nano **3**, 853–864 (2009).
[8] T. Huang, J. Zhao, M. Feng, H. Petek, S. Yang, and L. Dunsch, Phys. Rev. B **81**, 085434 (2010).
[9] G. Grancini, M. Maiuri, D. Fazzi, A. Petrozza, H.-J. Egelhaaf, D. Brida, G. Cerullo, and G. Lanzani, Nature Mater. **12**, 29–33 (2012).
[10] M. Kjellberg, O. Johansson, F. Jonsson, A. V. Bulgakov, C. Bordas, E. E. B. Campbell, and K. Hansen, Phys. Rev. A **81**, 023202 (2010).
[11] C. Bordas, F. Paulig, H. Helm, and D. L. Huestis, Rev. Sci. Instrum. **67**, 2257–2268 (1996).
[12] G. M. Roberts, J. L. Nixon, J. Lecointre, E. Wrede, and J. R. R. Verlet, Rev. Sci. Instrum. **80**, 053104 (2009).
[13] J. O. Johansson, J. Fedor, M. Goto, M. Kjellberg, J. Stenfalk, G. Henderson, E. E. B. Campbell, and K. Hansen, J. Chem. Phys. **136**, 164301 (2012).
[14] M. Tchaplyguine, K. Hoffmann, O. Duhr, H. Hohmann, G. Korn, H. Rottke, M. Wittmann, I. V. Hertel, and E. E. B. Campbell, J. Chem. Phys. **112**, 2781–2789 (2000).
[15] J. Cooper and R. N. Zare, J. Chem. Phys. **48**, 942–943 (1968).
[16] K. L. Reid, Annu. Rev. Phys. Chem. **54**, 397–424 (2003).
[17] M. J. Frisch, G. W. Trucks, H. B. Schlegel *et al.*, GAUSSIAN 09, Revision A.1, Gaussian, Inc., Wallingford, CT, 2009.
[18] A. Lassesson, K. Hansen, M. Joensson, A. Gromov, E. E. B. Campbell, M. Boyle, D. Pop, C. P. Schulz, I. V. Hertel, A. Taninaka, and H. Shinohara, Eur. Phys. J. D **34**, 205–209 (2005).
[19] K. Hansen, K. Hoffmann, and E. E. B. Campbell, J. Chem. Phys. **119**, 2513–2522 (2003).
[20] M. Kjellberg, A. V. Bulgakov, M. Goto, O. Johansson, and K. Hansen, J. Chem. Phys. **133**, 074308 (2010).
[21] J. L. Gosselin and P. M. Weber, J. Phys. Chem. A **109**, 4899–904 (2005).
[22] V. Blanchet, K. Raffael, G. Turri, B. Chatel, B. Girard, I. A. Garcia, I. Wilkinson, and B. J. Whitaker, J. Chem. Phys. **128**, 164318 (2008).
[23] P. Piecuch, J. A. Hansen, D. Staedter, S. Faure, and V. Blanchet, J. Chem. Phys. **138**, 201102 (2013).